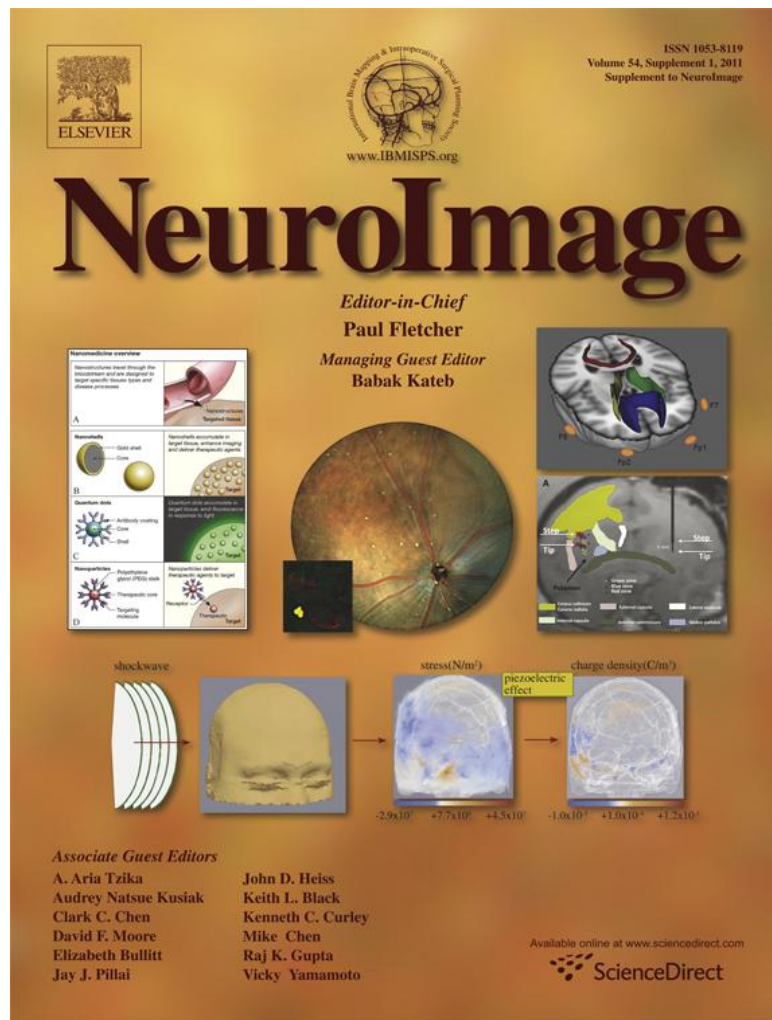


Provided for non-commercial research and education use.
Not for reproduction, distribution or commercial use.



This article appeared in a journal published by Elsevier. The attached copy is furnished to the author for internal non-commercial research and educational use, including for instruction at the author's institution and sharing with colleagues.

Other uses, including reproduction and distribution, or selling or licensing copies, or posting to personal, institutional or third party websites are prohibited.

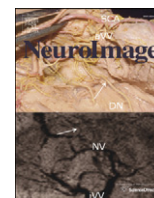
In most cases authors are permitted to post their version of the article (e.g. in Word or Tex form) to their personal website or institutional repository. Authors requiring further information regarding Elsevier's archiving and manuscript policies are encouraged to visit:

<http://www.elsevier.com/copyright>



Contents lists available at ScienceDirect

NeuroImage

journal homepage: www.elsevier.com/locate/ynimg

Identification of amyloid plaques in retinas from Alzheimer's patients and noninvasive *in vivo* optical imaging of retinal plaques in a mouse model

Maya Koronyo-Hamaoui ^{a,*}, Yosef Koronyo ^{a,f,1}, Alexander V. Ljubimov ^b, Carol A. Miller ^c, MinHee K. Ko ^a, Keith L. Black ^a, Michal Schwartz ^{d,2}, Daniel L. Farkas ^{e,f,*}

^a Department of Neurosurgery and Maxine Dunitz Neurosurgical Research Institute, Cedars-Sinai Medical Center, Los Angeles, CA, USA

^b Ophthalmology Research Laboratories, Cedars-Sinai Medical Center, and David Geffen School of Medicine at UCLA, Los Angeles, CA, USA

^c Departments of Pathology, Neurology and Program in Neuroscience, Keck School of Medicine, University of Southern California, Los Angeles, CA, USA

^d Department of Neurobiology, The Weizmann Institute of Science, Rehovot, Israel

^e Department of Biomedical Engineering, University of Southern California, Los Angeles, CA, USA

^f Departments of Surgery and Biomedical Sciences and Minimally Invasive Surgical Technologies Institute, Cedars-Sinai Medical Center, Los Angeles, CA, USA

ARTICLE INFO

Article history:

Received 14 April 2010

Revised 4 June 2010

Accepted 7 June 2010

Available online 13 June 2010

Keywords:

Human Retina

A β deposit

A β plaque

Alzheimer's disease

Mild cognitive impairment

Vaccination

Curcumin

In vivo optical imaging

Fluorescence

Spectral classification

ABSTRACT

Noninvasive monitoring of β -amyloid (A β) plaques, the neuropathological hallmarks of Alzheimer's disease (AD), is critical for AD diagnosis and prognosis. Current visualization of A β plaques in brains of live patients and animal models is limited in specificity and resolution. The retina as an extension of the brain presents an appealing target for a live, noninvasive optical imaging of AD if disease pathology is manifested there. We identified retinal A β plaques in postmortem eyes from AD patients ($n = 8$) and in suspected early stage cases ($n = 5$), consistent with brain pathology and clinical reports; plaques were undetectable in age-matched non-AD individuals ($n = 5$). In APP_{SWE}/PS1 Δ E9 transgenic mice (AD-Tg; $n = 18$) but not in non-Tg wt mice ($n = 10$), retinal A β plaques were detected following systemic administration of curcumin, a safe plaque-labeling fluorochrome. Moreover, retinal plaques were detectable earlier than in the brain and accumulated with disease progression. An immune-based therapy effective in reducing brain plaques, significantly reduced retinal A β plaque burden in immunized versus non-immunized AD mice ($n = 4$ mice per group). In live AD-Tg mice ($n = 24$), systemic administration of curcumin allowed noninvasive optical imaging of retinal A β plaques *in vivo* with high resolution and specificity; plaques were undetectable in non-Tg wt mice ($n = 11$). Our discovery of A β specific plaques in retinas from AD patients, and the ability to noninvasively detect individual retinal plaques in live AD mice establish the basis for developing high-resolution optical imaging for early AD diagnosis, prognosis assessment and response to therapies.

© 2010 Elsevier Inc. All rights reserved.

Introduction

Alzheimer's disease (AD) is a common and devastating age-dependent neurodegenerative condition. At present, a definite diagnosis of AD is determined after brain autopsy by detecting accumulation of the hallmark proteolytic products of amyloid precursor protein (APP), β -amyloid peptides (A β), which form extracellular aggregates termed A β plaques, and by the presence of

intracellular neurofibrillary tangles (Hardy and Selkoe, 2002; Sisodia and Price, 1995). A β plaques are believed to contribute to disrupted cellular activities and communication in the brain, leading to neurotoxic inflammation and neuronal death (McGeer and McGeer, 2002; Wyss-Coray, 2006). Major efforts have been invested in developing tools to enable noninvasive detection of amyloid plaques (e.g., through the skull) in living AD patients and animal models (Hintersteiner et al., 2005; Klunk et al., 2004; Nakada et al., 2008; Ng et al., 2007). However, such noninvasive monitoring of A β plaques is still clinically challenging, and is of limited resolution and availability (Klunk et al., 2005; Lockhart et al., 2007; Toyama et al., 2005). Optical detection constitutes a powerful, high-resolution and specific tool for *in vivo* imaging (Fujimoto and Farkas, 2009), as demonstrated using multiphoton microscopy to detect A β plaques in the mouse brain via an invasive cranial window (Meyer-Luehmann et al., 2008).

An alternative noninvasive approach to visualize amyloid plaques in AD patients at high resolution could be a direct optical imaging of the retina, provided that A β plaques are formed in patients' retinas and share properties with those in the brain. Choosing the retina as a

* Corresponding authors. M. Koronyo-Hamaoui is to be contacted at Departments of Neurosurgery and Biomedical Sciences, the Maxine Dunitz Neurosurgical Institute, Davis Research Building, Cedars-Sinai Medical Center, 8700 Beverly Boulevard, Los Angeles, CA 90048, USA. D.L. Farkas, New address: The Brain Window, Inc., 2049 Century Park East, Suite 3670, Los Angeles CA 90067.

E-mail addresses: maya.koronyo@cshs.org (M. Koronyo-Hamaoui), dlfarkas@gmail.com (D.L. Farkas).

¹ These authors contributed equally to this study.

² These authors contributed equally to this study.

target for visualization of brain disease also relies on it being a direct extension of the brain, having the potential to faithfully reflect AD brain's pathology. Retinal abnormalities in AD patients, some of which were detected at early stages, have been described in the past (Berisha et al., 2007; Blanks et al., 1996; Hinton et al., 1986; Katz and Rimmer, 1989; Sadun et al., 1987; Trick et al., 1989). These changes, however, mostly related to the nerve fiber layer (NFL) thickness reduction, seem to appear in additional pathologies of the eye and the brain including ocular hypertension, glaucoma, demyelinating optic neuritis, multiple sclerosis, and Parkinson's disease (Jindahra et al., 2010; Parisi, 2003). Detection of ganglion cell death in retinas of live AD mouse models has been recently documented (Cordeiro et al., 2010); however, this phenomenon is common to multiple neurodegenerative disorders including glaucoma and age-related macular degeneration. In addition, postmortem lenses from AD patients were reported to exhibit specific cytosolic nanometer-size A β aggregates and supranuclear cataracts in the peripheral lens (Goldstein et al., 2003). Encouraging results in APP_{SWE} and Presenilin (PS) 1 Δ E9 transgenic mice carrying the human mutated genes causing an early-onset familial AD were recently reported: these mice were found to develop human A β deposits in their retinal tissues at advanced stages of the disease (Ning et al., 2008; Perez et al., 2009).

The existing reports emphasized the need for unequivocal identification of A β plaque hallmark pathology of Alzheimer's disease in AD patients, especially at an early stage, for noninvasive *in vivo* detection of retinal plaques, and demonstration of their response to therapeutic intervention. Here, we report the presence of A β plaques in retinas of postmortem eyes from AD patients, and moreover, in retinas from those suspected as early stage cases. Using the APP_{SWE}/PS1 Δ E9 transgenic (AD-Tg) mice, we provide evidence for the formation of A β plaques in the retina prior to their manifestation in the brain. Further, in these mice we found that an immune-based therapy, using a weak agonist of a myelin-derived peptide loaded onto dendritic cells (Koronyo-Hamaoui et al., 2009), was effective in reducing A β plaques in the retinas to an extent similar to that observed in the brain. Importantly, we were able to demonstrate that systemic injection of curcumin (diferuloylmethane), a natural and safe fluorochrome that binds and labels A β plaques (Garcia-Alloza et al., 2007; Yang et al., 2005), into live AD mice allows high-resolution and specific noninvasive *in vivo* visualization of retinal A β plaques.

Materials and methods

Mice

Double transgenic mice (females and males in equal numbers) harboring the chimeric mouse/human APP (APP_{SWE}) and mutant human presenilin 1 (PS1 Δ E9) genes, and their aged-matched wt littermates, were purchased from the Jackson Laboratories (Bar Harbor, ME, strain #4462). Both APP_{SWE} and PS1 Δ E9 mutations are associated with early-onset Alzheimer's disease, and their expression is directed to CNS neurons. The "humanized" APP_{SWE} transgene allows the mice to produce and secrete a human A β peptide. All mice were bred and maintained in the Department of Comparative Medicine at Cedars-Sinai Medical Center. All experiments were approved and conducted according to the standards of the Cedars-Sinai Institutional Animal Care and Use Committee (IACUC).

Genotyping

Genomic DNA was extracted from 0.3 cm tail tip using a DNA extraction kit (Qiagen, Valencia, CA) following the manufacturer's protocol. Mice used in this study were genotyped for the presence of the transgenes by PCR, as previously described (Jankowsky et al., 2004b).

Immunization preparations

Mice were immunized with an altered myelin oligodendrocyte glycoprotein peptide [MOG45D; MEVGWYRSPFDRVHLYRNGK (Ford and Evavold, 2004)] that was derived from the pMOG_(35–55), in which aspartic acid is substituted for serine resulting in a non-encephalitogenic peptide. For immunizations, MOG45D (Invitrogen, Carlsbad, CA) was added to bone marrow-derived dendritic cells isolated from wt littermates. Preparation of dendritic cells for immunization was performed as previously described (Koronyo-Hamaoui et al., 2009).

Experimental design for immunization in mice

For immunization, 7-month-old mice were randomly divided into three treatment groups ($n = 4$ per group): AD-Tg mice injected with DC loaded with MOG45D peptide [0.5×10^6 cells/200 μ l in phosphate-buffered saline (PBS) per animal], once a month for 3 months; AD-Tg mice injected with PBS in the same regimen; and non-treated non-Tg wt littermates. At the end of the study, mice were perfused under anesthesia with ice-cold PBS. Brains and eyes were collected for further quantitative analysis of A β -plaque load.

Histology preparation of eyes and brains from mice

Both PBS-perfused and non-perfused animals were used in this study. For whole-eye cryosections, eyes were enucleated and fixed immediately in 4% paraformaldehyde (PFA) overnight at 4° C. Whole eyes were then placed in 30% sucrose solution and 2.5% PFA for 2 h, then washed three times for 15 min in PBS. The eyes were embedded in O.C.T. compound (Sakura Finetech, Torrance, CA), frozen gradually on dry ice, and sagittally cryosectioned (7 μ m). For whole-mount retinas, the anterior eye portion was dissected out, eyecups were soaked for 10 min in hyaluronidase (type I-S) (0.07 mg/ml) (Sigma-Aldrich, St. Louis, MO) to liquefy and remove the vitreous residue, and then washed three times for 10 min in PBS. Eyecups were then fixed with 2.5% PFA overnight at 4° C. Retinas were dissected free and whole-mounts were prepared flat on slides. For brain cryosections, brains were collected and fixed immediately in 2.5% PFA overnight at 4° C. Brains were then transferred into 30% sucrose in 2.5% PFA for 2 days, washed three times for 15 min in PBS, embedded in O.C.T. and frozen gradually on dry ice, then coronally cryosectioned (30 μ m).

Human subjects

Postmortem eyes and brains were obtained from the USC Alzheimer's Disease Research Center (ADRC) Neuropathology Core (IRB approval #042071), Department of Pathology, University of Southern California (Los Angeles, CA), and also purchased from National Disease Research Interchange (NDRI, Philadelphia, PA), under IRB protocols # 99491 and # 3201. NDRI maintains a human tissue collection protocol approved by a managerial committee and subject to National Institutes of Health oversight. Postmortem specimens were collected from patients with a definite AD diagnosis ($n = 8$; average age 80 years, ranging from 48 to 94 years; with different disease severities, categorized based on their neuropathology reports), patients with a possible or probable AD diagnosis ($n = 5$, average age 79 years, ranging from 65 to 92 years), and from age-matched normal controls ($n = 5$; average age 76 years, ranging from 66 to 85 years, with absence of dementia and brain pathology; human donor eye records are summarized in Table S1). The groups did not differ significantly in age or years of education.

Assessment of human AD diagnosis and cognitive evaluation

Clinical and neuropathology reports, including neurological examination, neuropsychological testing, such as cognitive assessment, family history and medications, were provided by the USC ADRC Clinical Core (IRB protocol # 002003). Each participant had been tested individually by a trained psychometrist under the supervision of a licensed clinical neuropsychologist. Test scores from the evaluation closest to death were used in these analyses. Most cognitive evaluations were performed annually and in most cases, less than 1 year prior to death. Two global indicators of cognitive status were used for clinical assessment of patients, the Clinical Dementia Rating (CDR) and the Mini Mental Status Examination (MMSE: normal control = 30–26; MCI = 25–22; AD ≤ 22). For neuropathologic diagnoses, modified CERAD (Mirra et al., 1991) were used as well as the NIA/Reagan protocols (NIA-Reagan Consensus, 1997). This includes A β burden and neurofibrillary tangle pathology (NFT) assessments in multiple brain areas. Amyloid plaques and tangles in the brain were evaluated using the Thioflavin-S (ThioS) fluorescent and Gallyas silver stains in formalin-fixed, paraffin-embedded tissues. Scoring was performed by independent observations of three neuropathologists and an arbitrary score, reflecting amyloid or NFT burden as an average of all three readings (0 = none, 1 = sparse, 3 = moderate, 5 = abundant), was assigned to each individual. Braak scores were used to assess NFTs for disease progression.

Histology preparation of human postmortem eyes and brains

Postmortem eyes were fixed and long-term stored in 10% neutral buffered formalin (NBF). In addition, four eyes were snap frozen and stored at -80° C. No apparent differences were observed in immunostaining between the two preparation methods, except for DAPI staining that was clearer in the snap frozen eyes without long-term 10% NBF fixation. For immunohistochemistry, fresh-frozen brains were cryosectioned, fixed with 2.5% PFA for 2 days and stored in PBS at 4° C. The fresh-frozen eyecups were hyaluronidase-treated as above, to liquefy and remove vitreous residues, washed three times for 5 min in PBS, and fixed in 2.5% PFA for 2 days. Retinas were dissected free, and whole-mounts were prepared. The long-term NBF-fixed eyecups were washed in PBS, retinas were dissected free, vitreous was cleaned manually, and whole-mounts were prepared.

Immunohistochemistry in mouse tissues

Mouse brain cryosections (30 μ m), retinal cross-sections (7 μ m) and whole-mounted retinas were treated with a permeabilization/blocking solution containing 20% horse serum (Invitrogen) and 0.05% Triton X-100 (Sigma-Aldrich). Sections and whole-mounted retinas were stained overnight at 4° C with a specified combination of the following primary monoclonal antibodies (mAbs) in PBS containing 10% blocking solution: mouse anti-human A β [against human amino acid (aa) residues 1–16, clone 6E10 (1:100; Millipore, Temecula, CA), and clone DE2B4 (1:100; AbD Serotec, Raleigh, NC), and against the aa 17–24, clone 4G8 (1:100; Covance, Princeton, NJ), and mAbs directed against C-terminus of human A β , aa 34–40, clone 11A5-B10, specific for isoforms ending at 40th aa (1:100; Millipore; does not cross-react with APP) and against C-terminus of human A β , aa 36–42, clone 12F4, specific for isoforms ending at 42nd aa (1:200; Covance; does not cross-react with APP)]; rabbit anti-mouse A β [against mouse aa 3–16, and reacting only with mouse or rat, Ab14220 (1:500; Abcam, Cambridge, MA)]. Next, sections were incubated for 1 h at room temperature with secondary Abs in PBS (Cy5-conjugated donkey anti-mouse antibody or donkey anti-rabbit antibody; 1:200; Jackson ImmunoResearch Laboratories, West Grove, PA), washed three times with PBS, and a Vectashield mounting solution with or without 4',6-diamidino-2-phenylindole dihydrochloride (DAPI; Vector Labo-

ratories, Burlingame, CA) was applied. Routine controls were processed using the same protocol with the omission of the primary antibody.

Immunohistochemistry in human tissues

Human brain cryosections (30 μ m) and whole-mount retinas from AD patients and controls were treated with target retrieval solution (Dako, Carpinteria, CA) and with a permeabilization/blocking solution (as mentioned before). All human tissues were treated with Sudan Black B (SBB) to eliminate background fluorescence. Human tissues were stained with primary mAbs mentioned above, in PBS containing 10% blocking solution, for 48 h at 4° C. The samples were incubated for 1.5 h at room temperature with secondary Abs (as mentioned before) in PBS, and washed three times with PBS. Next, labeled samples were immersed for 10 min in 70% ethanol (v/v) supplemented with 0.3% (w/v) SBB, followed by three washes with 70% ethanol (v/v) and finally with PBS. After staining with SBB (Sigma-Aldrich; C₂₆H₂₄N₄O, a lysochrome used for staining of neutral triglycerides and lipids), the same fluorescently labeled samples were stained with curcumin or ThioS (see separate sections below) and then mounted with or without DAPI. Alternatively, A β immunoreactivity was detected with 12F4 mAb and was visualized by nonfluorescent immunoperoxidase method using 3,3'-diaminobenzidine as the chromogen (DAB substrate, Sigma-Aldrich) and Vectastain ABC kit (Vector Laboratories) as specified by the manufacturer. Routine controls were processed using the same protocol with the omission of the primary antibody to assess nonspecific labeling.

Thioflavin-S staining

ThioS solution at 1% (w/v) was prepared by dissolving 1 g Thioflavin-S (Sigma-Aldrich) in 70% ethanol (v/v). Mouse whole-mounted retinas were stained for 12 min at room temperature, then dipped three times in 70% ethanol (v/v) and finally washed once in PBS. The samples were covered with mounting media without DAPI (Vector Laboratories). Human whole-mount retinas were first stained with SBB and washed three times with PBS for 5 min each wash. Samples were then stained with ThioS solution, dipped three times in 70% ethanol (v/v), finally washed once in PBS, and mounted as mentioned above.

Ex vivo curcumin staining

Curcumin solution was prepared by dissolving 2 mg curcumin (Sigma-Aldrich) in two drops of 0.5 M NaOH (vigorous vortex mixing), followed by immediate dissolution and dilution in PBS to achieve a final concentration of 0.1 mg/ml (pH = 7.9). Human whole-mounted retinas and brain sections were initially treated with 0.3% (w/v) SBB in 70% ethanol (v/v) for 10 min at room temperature. All mouse and human tissues (brain and retinal cryosections and/or whole-mounts) were stained with curcumin solution for 10 min at room temperature, and then washed three times with PBS for 15 min each. The samples were covered with ProLong Gold antifade mounting media with DAPI (Invitrogen) or Vectashield (Vector Laboratories) with or without DAPI.

Intravenous injections of curcumin for ex vivo plaque imaging

AD-Tg ($n = 18$) and non-Tg (wt; $n = 10$) mice were i.v. injected into the tail vein with curcumin in PBS (7.5 mg/kg/day) or with PBS alone, for 5 consecutive days. Subsequently, brains and eyes were excised, and brain cryosections and retinal whole-mounts were prepared for imaging.

Intravenous injections of curcumin for noninvasive *in vivo* retinal plaque imaging

Retinas of live AD-Tg ($n=24$) and wt ($n=11$) mice were imaged following systemic administration of curcumin (7.5 mg/kg/day), for 5 consecutive days or following a single i.v. injection 2 h prior to imaging. Mice were anesthetized with 70 mg/kg ketamine and 30 mg/kg xylazine. Mouse pupils were dilated to about 2 mm in diameter with 0.5% phenylephrine hydrochloride ophthalmic solution (Bausch & Lomb, Rochester, NY) combined with 0.5% tropicamide ophthalmic solution (Mydral, Bausch & Lomb). Mouse eyes were covered with a drop of Gonak (Hypromellose ophthalmic demulcent solution, 2.5%; Akorn, Lake Forest, IL), which served as an optical coupling medium, and the retinas were imaged *in vivo* using the Micron II retinal imaging microscope (Phoenix Research Laboratories, San Ramon, CA). The Micron II is a retinal imaging microscope for rodents adjusted to visualize fluorescence signals at high resolution and is equipped with a 3-CCD camera (1000 to 1 dynamic range and 30 frames per second output at XGA resolution), and specific set of filters suitable to detect curcumin fluorescence (as mentioned below for the Zeiss Axio Imager Z1). Images were repeatedly captured at several angles of the retina in order to visualize a larger field and eliminate non-specific reflection signals. Care was taken to keep anesthetized animals warm throughout the procedure.

Microscopy

Fluorescence and bright-field images were acquired using a Carl Zeiss Axio Imager Z1 fluorescence microscope equipped with ApoTome (Carl Zeiss MicroImaging, Inc.), and a Leica TCS SP5 double-spectral confocal microscope, using the same setting and exposure times for each experiment. For processing and analysis of the images, the AxioVision (Rel. 4.6.3) software (Carl Zeiss) was used. Fluorescence in the Zeiss Axio Imager Z1 was imaged using filter sets for excitation and emission at 365/50 and 445/50 nm for DAPI, 470/40 and 525/50 nm for ThioS, 550/25 and 605/70 nm for curcumin, and 640/30 and 690/50 nm for Cy5. In the presented images, curcumin was assigned a green pseudocolor to differentiate from red Cy5.

Quantification

Images of stained tissues were obtained on an Axio Imager Z1 microscope (with motorized Z-drive) with AxioCam MRm monochrome camera ver. 3.0 (at a resolution of 1388×1040 pixels, $6.45 \mu\text{m} \times 6.45 \mu\text{m}$ pixel size, dynamic range of $>1:2,200$, that delivers low-noise images due to Peltier-cooled sensor). Quantitative analysis of A β plaque number and area (μm^2) was performed from two whole-mounted retinas per mouse ($n=4$ mice per group). Each image, captured with 40x objectives with resolution of $0.25 \mu\text{m}$, included an area of 0.04 mm^2 , and a total of 12 rectangle areas around the optic disc within scanning depth of $60 \mu\text{m}$ (multiple virtual section images at consecutive focal planes using a motorized scanning stage). Measurements of the average plaque radius (following curcumin staining) were completed for each animal group followed by calculation of the average plaque area in each animal group. For the acquisition, we used the same exposure times (approx. 75 ms) and the same gain values (0) for all images. The emission signals of A β plaques stained with curcumin were compared to the background signals in the retinal tissue, to determine signal-to-background ratio. The calculated signal-to-background noise ratio from the images was high and within the range of 3:1 to 10:1. Quantification of A β plaque number and area in the corresponding brains was performed using three coronal sections (two hemispheres each) per mouse in 450 μm intervals, over an area covering the hippocampus and cortex regions. Optical sections from each field of the specimen were imported into the NIH ImageJ program (National Institutes of Health). Conversion to grayscale was performed to distinguish between areas of immuno-

reactivity and background. Total area of immunoreactivity was determined using a standardized histogram-based threshold technique, and then subjected to particle analysis.

Spectral imaging analyses

Spectral imaging of mouse retinal tissues provided digital images of an object at a large, sequential number of wavelengths and generated precise optical signatures at every pixel. The fluorescence spectral signature of A β plaques labeled *in vivo* with curcumin was captured by our spectral imaging system using the following equipment: Nikon fluorescence microscopes (E800 and TE2000) with mercury and xenon arc lamps, a CCD camera, and an AOTF (acousto-optic tunable filters)-based spectral image acquisition system ($\sim 4 \mu\text{m}$ spectral resolution, commercialized by ChromoDynamics, Inc., Orlando, FL) (Wachman et al., 1997). Image acquisition was followed by image segmentation and classification using software that we previously developed (Burton et al., 2009). The final images provided a visual pseudocolor representation of the spectral signature extracted from the raw images, representing the size and location of the analyzed objects. Spectral analysis of individual A β plaques (regions of interest, ROI) as compared to background signals in human retinal tissues (single labeled with curcumin, single labeled with Cy5-conjugated Abs, or double labeled with both) was performed in quadruplicates using a Leica TCS SP5 double-spectral (excitation and emission) confocal microscope, with the same setting and exposure times for each ROI. Various excitation wavelengths and resulting emission spectra (at 5 nm intervals) were recorded, to determine the optimal wavelengths to excite and capture the fluorescence signal. GraphPad Prism 5 for Mac OS X version 5.0b was used to smooth curves by applying the fit spline/lowess method.

Statistical analysis

GraphPad Prism 5.0b (GraphPad Software, San Diego, CA) was used to analyze the data. Comparison of means between the three experimental groups (PBS-treated vs. immunized AD-Tg and non-Tg wt mice) was performed by one-way analysis of variance (ANOVA) followed by Bonferroni multiple comparison post-test analysis to define specific *P* value of each group pair. Results are expressed as mean and \pm SEM. $P < 0.05$ was considered significant.

Results

Curcumin binds to retinal A β plaques in a mouse model of Alzheimer's disease

We first assessed the potential of using curcumin for the development of an *in vivo* noninvasive method to detect retinal A β plaques. To this end, we first verified that curcumin could specifically *ex vivo* label A β plaques in the retinas of AD-Tg mice. Retinal whole-mounts and cross-sections from AD-Tg and non-Tg (wt) mice were co-stained with curcumin and four different anti-A β mAbs (Fig. 1). Retinal A β plaques, co-labeled with curcumin and 11A5-B10 or 12F4 mAbs [recognizing the C-terminal amino acid sequence of A β_{40} and A β_{42} isoforms, respectively], were virtually absent in non-Tg (wt) littermates (Fig. 1a and d), whereas they were clearly detected in AD-Tg mice (Fig. 1b, c, e, and f). Staining with anti-A β_{42} mAb resulted in stronger fluorescence signal than with the anti-A β_{40} mAb (Fig. 1c' vs. 1f'), in agreement with the reported brain A β_{40} :A β_{42} ratio of 1:2 in this mouse model (Jankowsky et al., 2004a). Additional staining with ThioS that labels mature/fibrillar A β plaques (Fig. S1a–c), demonstrated a staining pattern and size of retinal A β plaques very similar to curcumin labeling; both dyes were reported to bind the β -pleated sheet structures of A β plaques (Garcia-Alloza et al., 2007; Goldstein et al., 2003). The specificity of curcumin-labeled A β plaques in the

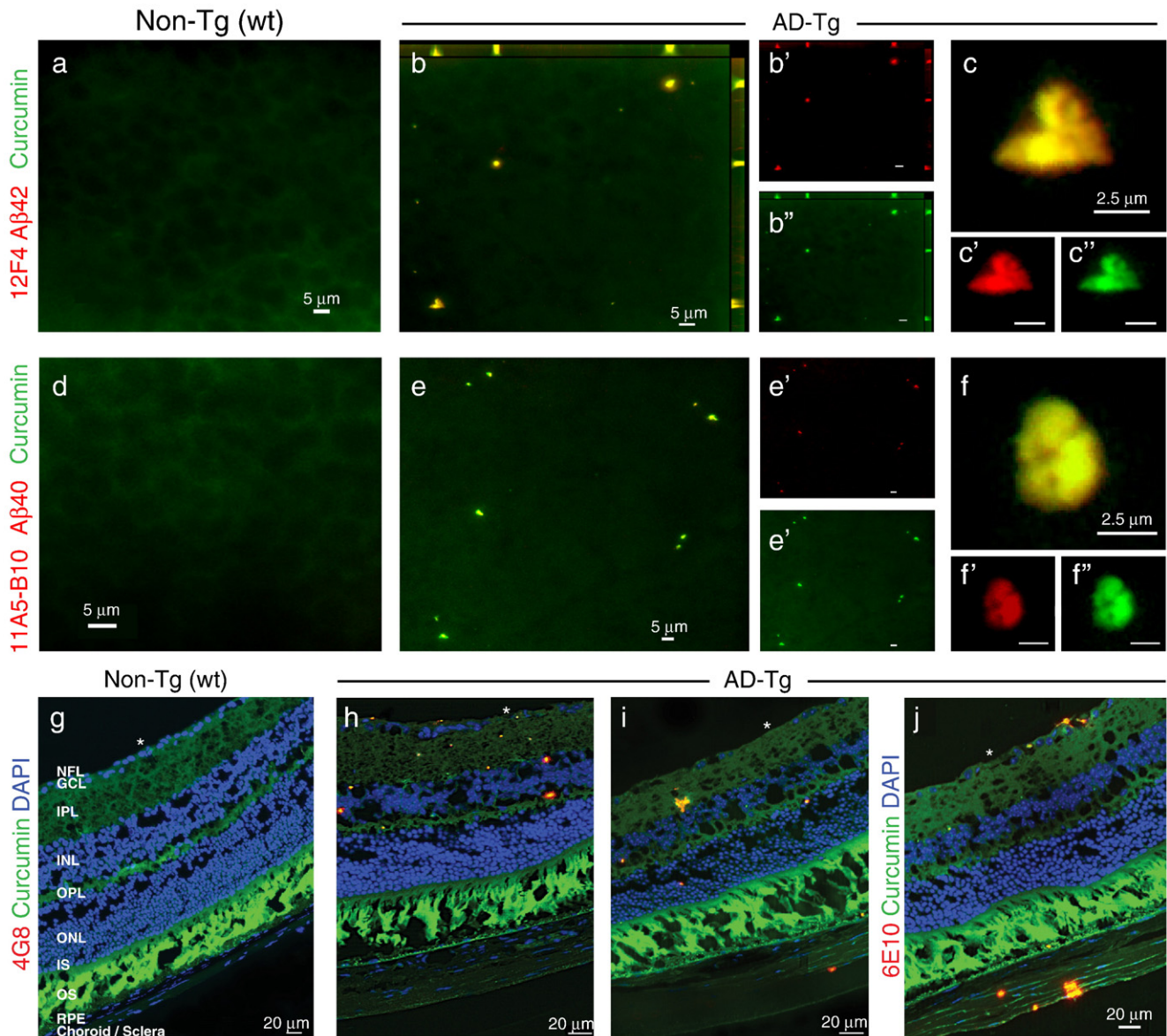


Fig. 1. Detection of retinal A β plaques in AD-Tg mice by *ex vivo* curcumin labeling. Whole-mounted retinas and whole-eye sagittal cryosections from 10-month-old non-Tg (wt) and AD-Tg mice stained with various anti-human A β mAbs (12F4, 11A5-B10, 4G8 and 6E10; secondary Ab-Cy5 conjugate; red color) and curcumin (green color). Double-labeled A β plaques appear in yellow color. (a–c) Representative images of whole-mount retinas double-stained with curcumin and A β ₄₂ mAb (12F4; specific to the C-terminal sequence ending at aa 42). (a) No retinal A β plaques were detected in wt mice, whereas (b) they were found in AD-Tg mice; here and below, whenever z-axis projection images are presented, the axes ZY and ZX are shown on the top and right side of the image. (c) Specific staining patterns of A β ₄₂-containing retinal plaques at a higher magnification; (b'–c'') Separate channels for each staining; (d–f) Whole-mount retinas double-stained with anti-human A β ₄₀ mAb (11A5-B10; specific to the C-terminal sequence ending at aa 40) and curcumin. (d) No detection of A β plaques in wt mice. (e) Specific A β plaques were found in AD-Tg mice. (f) Higher magnification image demonstrating A β ₄₀-containing plaques and their specific staining pattern. (e'–f'') separate channels. (g–j) Whole-eye cross-sections stained with anti-A β mAbs (4G8 or 6E10), curcumin and DAPI nuclei staining. (g) No evidence for double-positive curcumin and anti-human A β plaques in wt mice. (h–j) Curcumin-positive A β plaques co-labeled with 4G8 or 6E10 were identified in various retinal layers, including the GCL-ganglion cell layer, IPL-inner plexiform layer, INL-inner plexiform layer, OPL-outer plexiform layer and ONL-outer nuclear layer; (i and j) A β plaques were also detected in the sclera. White asterisks indicate DAPI nuclear staining in the GCL: undamaged in wt retinas and deficient in retinas from AD-Tg mice.

mouse retina was further confirmed with 4G8 and 6E10 antibodies in cross-sections (Fig. 1g–j). In line with previous data using ThioS/10D5 antibody (Ning et al., 2008; Perez et al., 2009), curcumin-positive retinal A β plaques were specifically found in AD-Tg mice (Fig. 1h–j) in various locations including the nerve fiber layer (NFL), retinal ganglion cell layer (RGC), inner (IPL) and outer (OPL) plexiform layers, and inner nuclear layer (INL); some plaques were also seen in the sclera (Fig. 1i and j). Relatively high background fluorescence was observed in the photoreceptor outer segment (OS) layer of the retina, as this layer in the mouse displays an endogenous fluorescence; however, curcumin- and immuno-labeling of plaques appeared above

the autofluorescence levels and were easily distinguishable from these diffused background signals.

Specific curcumin in vivo labeling of A β plaques in AD mice and early plaque detection in the retina

To establish the use of curcumin for *in vivo* imaging of plaques in the retina, we tested its bioavailability to the eye when injected systemically. Labeled plaques following systemic administration of curcumin were detected in the retinas and brains of AD-Tg mice, but not of the wt controls (Fig. 2). These findings confirmed that

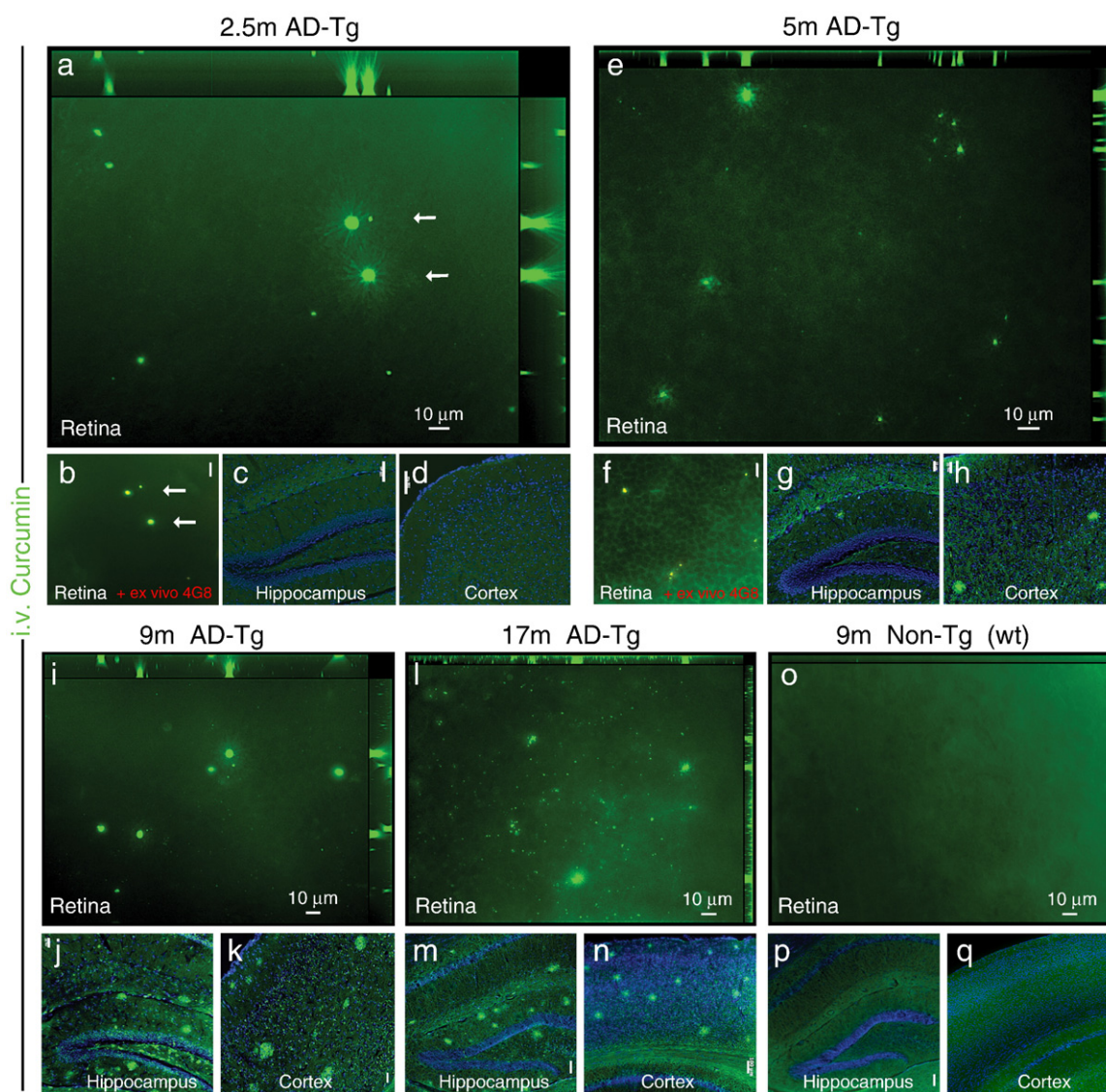


Fig. 2. Bioavailability of systemically administered curcumin to the mouse eye: accumulation of curcumin-labeled retinal A β plaques with disease progression and detection at early pre-symptomatic stage. (a–q) Representative z-axis projection images of whole-mount retinas and brain coronal cryosections from AD-Tg and non-Tg (wt) mice at various ages, following i.v. curcumin injections for 5 days: In 2.5-month-old AD-Tg mouse (a and b) retinal curcumin-labeled *in vivo* A β plaques (green) were visible, with further (b) validation of A β plaque identity in the same retinal location (arrows) by staining *ex vivo* with anti-human A β mAb 4G8 (secondary Ab-Cy5 conjugate). Co-localization of curcumin and A β antibody in yellow pseudocolor. Scale bar = 10 μ m. (c and d) No plaques were detected in the brain hippocampus and cortex of 2.5-month-old AD-Tg mice. Scale bars = 100 μ m. (e–h) 5-month-old AD-Tg mouse: (e) Presence of curcumin-labeled plaques in the retina and (f) co-labeling following 4G8 mAb staining *ex vivo*. Scale bar = 20 μ m; (g and h) detection of plaques in the brain. Scale bars = 50 μ m. (i–k) 9-month-old AD-Tg mouse: (i) Multiple plaques in the retina and (j,k) in the brain. Scale bars = 50 μ m. (l–n) 17-month-old AD-Tg mouse: (l) Numerous plaques in the retina and (m and n) in the brain. Scale bars = 100 μ m. (o–q) 9-month-old non-Tg (wt) mouse: (o) No A β plaques in the retina nor (p and q) in the brain. Scale bars = 100 μ m.

curcumin crosses the blood–brain barrier (Garcia-Alloza et al., 2007) and the blood–retina barrier and indicated its high affinity for A β plaques *in vivo*. Imaging of retina, brain cortex, and hippocampus of AD-Tg mice at the ages of 2.5, 5, 9, and 17 months demonstrated a qualitative age-dependent correlation between plaque deposition in the retina and the brain, and increased accumulation over the course of disease progression (Fig. 2a–n). Importantly, plaques were detected in the retina (Fig. 2a and b), but not in the brain (Fig. 2c and d), as early as at 2.5 months of age in AD-Tg mice, suggesting that A β plaques in the retina precede brain plaques. We further confirmed that these curcumin-labeled plaques were co-localized *ex vivo* with mAb 4G8 in the same tissue location (Fig. 2b). A β plaques were first detectable in the brain at the age of 5 months (Fig. 2g and h), in line with previous descriptions of disease initiation and progression in

this strain of AD-Tg mice (Garcia-Alloza et al., 2006). Retinal A β plaques, similar to plaques in the brain, were more frequently found in older AD-Tg mice, at the age of 9 and 17 months (Fig. 2i–n). As expected, plaques could not be detected in the retinas and brains of 9-month-old wt mice (Fig. 2o–q).

Reduction of retinal A β -plaque burden in AD mice following an immune-based therapy

To strengthen our contention of the retina as a viable, functional target for imaging AD, we investigated whether retinal plaques behaved similarly to brain plaques in response to the same therapy. We previously showed that immunization with an altered myelin-derived peptide [MOG45D, derived from pMOG_{35–55} (Ziv et al.,

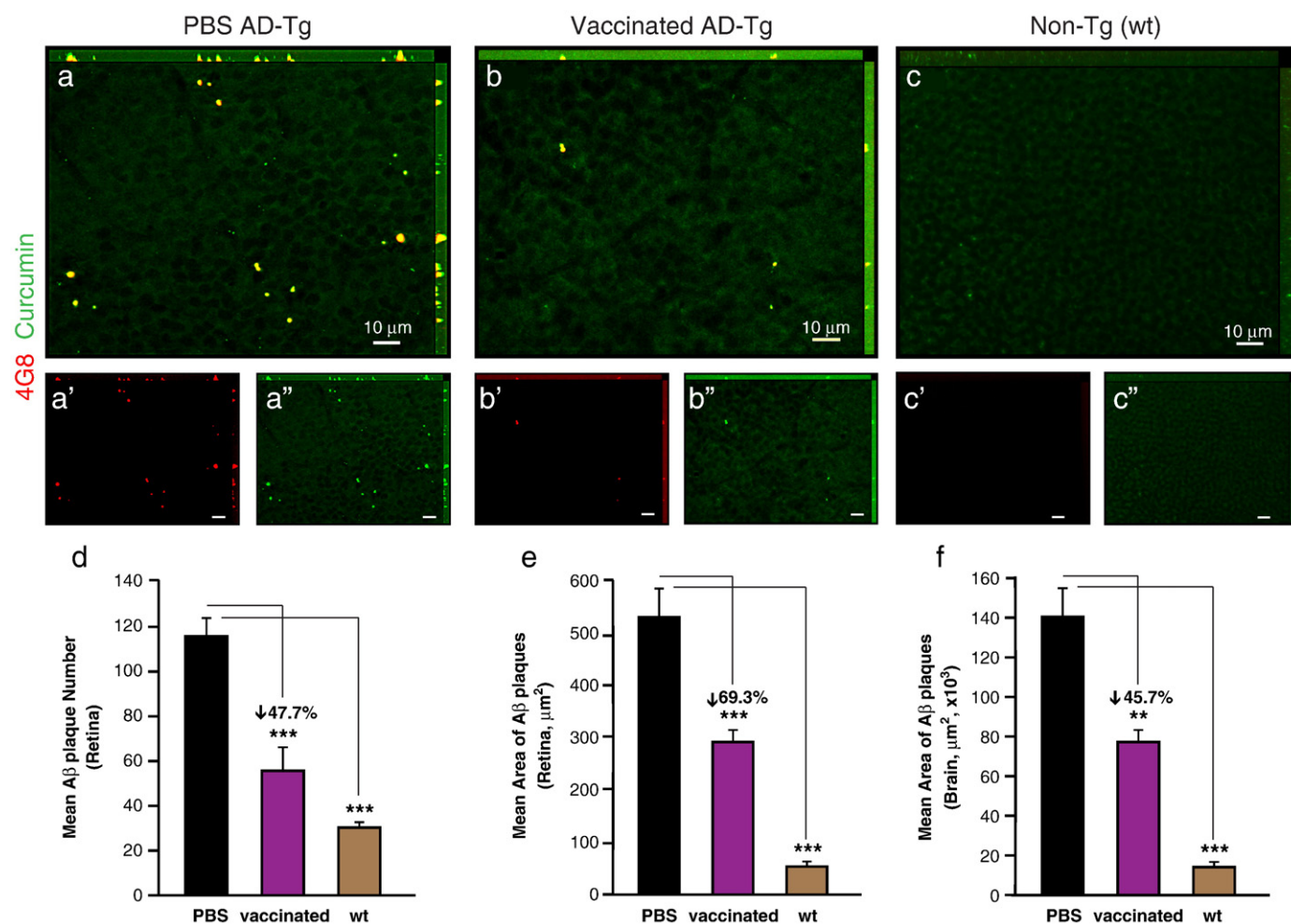


Fig. 3. Reduced A β -plaque burden in retinas from AD-Tg mice following MOG45D-loaded dendritic cells immunization. (a–c) Representative z-axis projection images of whole-mount retinas from (a) PBS-treated control and (b) MOG45D-vaccinated AD-Tg mice, and from (c) non-Tg (wt) mouse, stained *ex vivo* with curcumin and anti-human A β mAb (4G8; followed by secondary Ab-Cy5 conjugate). (d and e) Following MOG45D-loaded DCs vaccination, a significant reduction in mean curcumin-positive plaque number and area was observed in retinas from vaccinated AD-Tg mice as compared to PBS-treated controls. (f) A significant decrease in total area covered by plaques was detected in brain hippocampus and cortex from the same mice following the immunotherapy. Curcumin staining revealed the same decrease in plaque burden following vaccination in the retina and in the brain, while A β mAbs confirmed its specificity to A β , suggesting that curcumin is a suitable dye for monitoring A β plaque changes. Error bars represent SEM. Asterisks indicate statistical significance: *** P <0.0001; ** P <0.005, analyzed by one-way ANOVA followed by Bonferroni multiple comparison post-test.

2006)] loaded on dendritic cells (DCs), effectively restricted A β plaque burden in brains of AD-Tg mice (Koronyo-Hamaoui et al., 2009). We therefore used the same immunization to assess its effect on retinal plaques, while establishing curcumin as a potential fluorochrome to monitor plaque changes. Quantitative analysis of curcumin-labeled A β plaque number and area was performed on brain sections and whole-mounted retinas isolated from three experimental groups: 10-month-old MOG45D-immunized or PBS-treated AD-Tg mice and age-matched untreated wt controls (Fig. 3). A substantial reduction of retinal A β plaque burden by mean number and area was found in immunized AD-Tg mice compared to PBS-treated controls (representative images: Fig. 3b vs. a; quantitative analyses: Fig. 3d and e, P <0.0001). Notably, a significant decrease in total plaque area, relative to PBS-treated mice, was also observed in brain hippocampi and cortices of the same immunized AD-Tg mice (Fig. 3f; P <0.0001). No A β plaques (double labeled with curcumin and anti-human A β antibody) were detected in the wt mice, as they do not possess the human transgene (Fig. 3c). Whereas human A β -containing plaques were obviously absent in

the wt mice, occasional small and sparse curcumin-positive plaques ($\leq 1 \mu\text{m}$; anti-human A β negative) were detected at higher magnification. These small plaques, which were detected using curcumin in all three experimental groups, were co-labeled with the specific anti-mouse A β antibody (Fig. S2a–e), confirming their identity as endogenously formed mouse A β deposits.

Noninvasive imaging of curcumin-labeled retinal plaques in live AD mice

The results summarized above encouraged us to proceed to imaging plaques in live animals (Fig. 4). Following systemic administration of curcumin, *in vivo* imaging of the retina was performed in live mice utilizing Micron II rodent retinal imaging microscope. Retinal A β plaques were absent in curcumin-injected non-Tg (wt) mice (Fig. 4a and a') and in PBS-injected AD-Tg mice (not shown), whereas they were clearly identified in curcumin-injected live AD-Tg mice (Fig. 4b and b'). This *in vivo* optical imaging modality enabled us to identify individual plaques or plaque clusters at high resolution (Fig. 4b'). We confirmed the

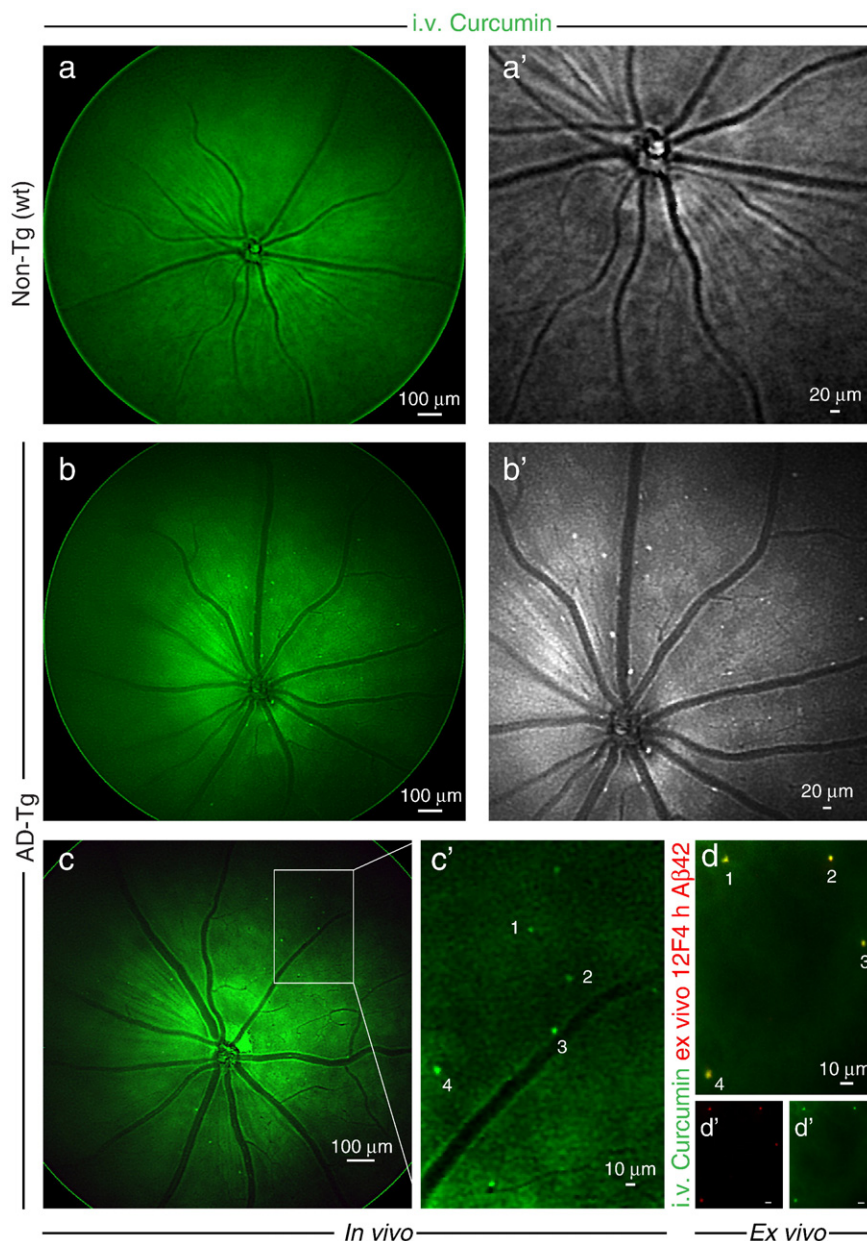


Fig. 4. Noninvasive *in vivo* optical imaging of curcumin-labeled A β plaques in AD-Tg mice retina. (a–c) Following *i.v.* administration of curcumin (7.5 mg/kg) for 5 consecutive days, retinas of 8- to 12-month-old AD-Tg and wt mice were *in vivo* fluorescently imaged using Micron II rodent retinal microscope. Representative *in vivo* mouse fundus images: (a) no plaques could be visualized in wt mouse; (a') higher magnification in grayscale. (b) Retinal curcumin-labeled plaques (green spots) were visible in live AD-Tg mouse; (b') higher magnification in grayscale. (c and c') Representative images demonstrate *in vivo* detection of curcumin-labeled plaques in the retinas of 8 month-old AD-Tg mice, following a single *i.v.* injection of curcumin (7.5 mg/kg) 2 h prior to imaging. (c') Enlarged image of the selected area from (c) demonstrates that this imaging modality enables the identification of individual plaques or plaque clusters at a high spatial resolution. Note that blood vessels appear unstained (dark), possibly due to blood flow in the live mouse. (d) Whole-mount retina prepared from the same *in vivo* imaged mouse eye as in (c), following perfusion. An additional *ex vivo* staining with anti-human A β_{42} mAb (12F4; secondary Ab-Cy5 conjugate) further confirmed the specificity of curcumin signals (captured by Micron II) to A β plaques. (d' and d'') separate channels for each staining. A similar pattern of curcumin-positive plaques imaged *in vivo* was identified *ex vivo* following antibody labeling (indicated by the numbers 1–4).

specificity of the signals captured in live mice by performing a new experiment in which we excised retinas following *in vivo* imaging of curcumin-labeled A β plaques (Fig. 4c and c'), and determined their identity *ex vivo* by staining with specific mAb 12F4 (Fig. 4d). Another *ex vivo* labeling with mAb 4G8 of an additional whole-mounted AD-Tg mouse retina, demonstrated the A β specificity of curcumin staining and that A β plaques could be found inside blood vessels (intraluminal) and especially in the abluminal position (Fig. S3a). Overall, average plaque size detected *in vivo* was very similar to that observed by immunostaining *ex vivo*.

We next identified the specific optical signature of retinal A β plaques in curcumin-injected non-perfused mice in order to further verify curcumin-labeled A β plaque detection and to reduce the possibility of monitoring non-specific signals emerging from non-plaque regions or background noise. For this purpose, we monitored plaques in the vicinity of blood vessels using a spectral optical imaging technology (Burton et al., 2009; Wachman et al., 1997). We detected both curcumin-labeled plaques and blood vessels in a single wavelength channel specific to curcumin (Fig. S3b). By applying band-sequential spectral image acquisition and spectral signature-

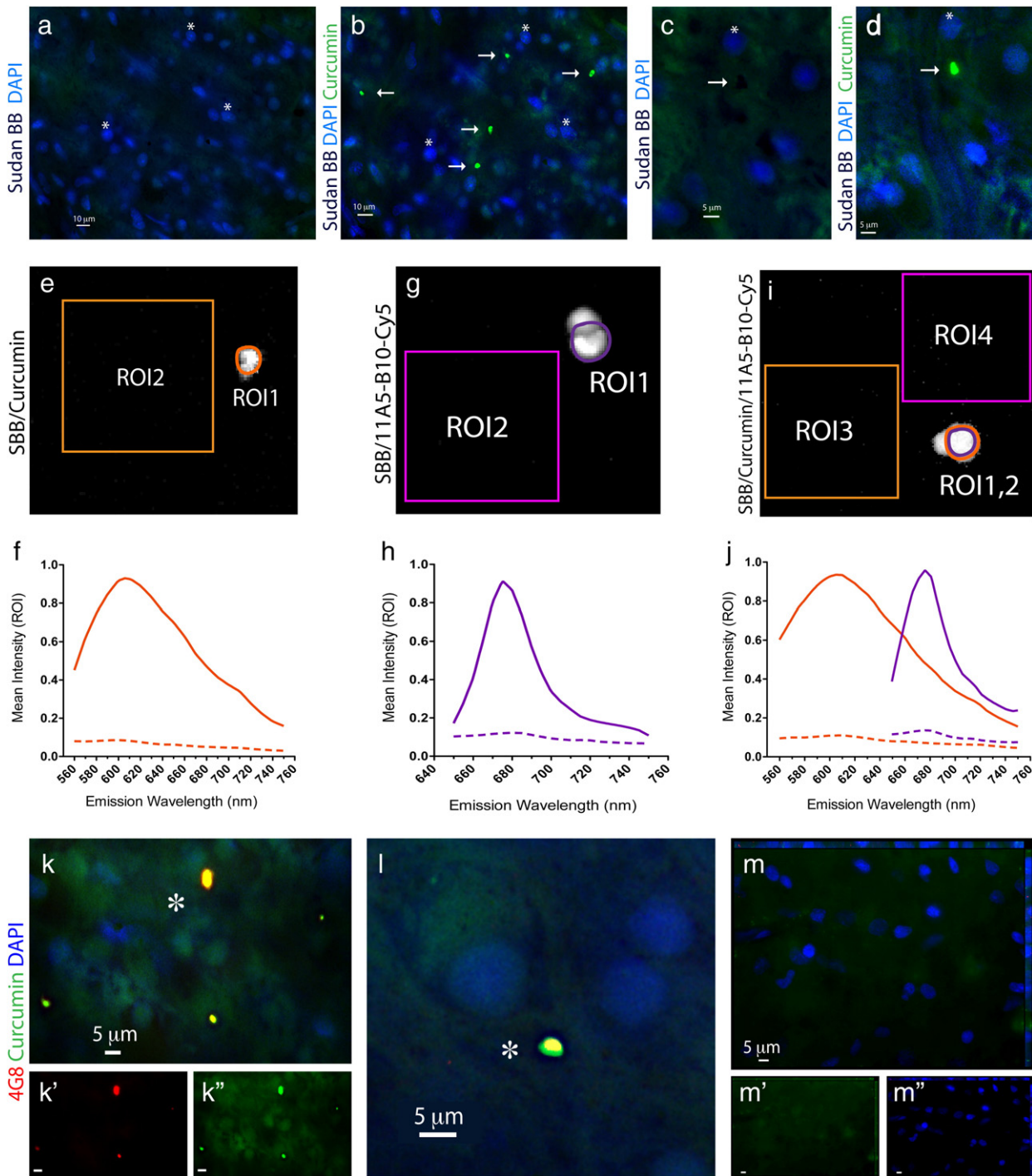


Fig. 5. Identification of A β plaques in the human retina from AD patients via a specific curcumin labeling. All stainings of human whole-mount retinas included a Sudan Black B (SBB) pretreatment to eliminate non-specific autofluorescence signals. (a–d) Whole-mounted retinas from human AD patients were first immersed with SBB and subsequently stained with curcumin and DAPI; (a and c) no plaques were observed after staining with SBB, whereas (b and d) subsequent staining of the same human retinas with curcumin revealed the presence of A β plaques (indicated by arrows; asterisks mark the nuclei of the same tissue location). (c and d) At higher magnification, dark spots of SBB staining are evident, and following curcumin staining a specific A β plaque signal is detected in the same retinal location. (e–j) Signal specificity of individual retinal A β plaques, single labeled with curcumin or with anti-A β ₄₀ (11A5-B10; secondary Ab-Cy5 conjugate), or double labeled with both, was confirmed by spectral image analysis performed in quadruplicates in a Leica TCS SP5 double-spectral confocal microscope. Regions of interest (ROI) were marked and their corresponding signal intensity was recorded at increasing emission wavelengths from 560 nm to 750 nm to create the spectral curves for A β plaques versus background. (e) Representative image of a single curcumin-labeled A β plaque in a retinal whole-mount (ROI1) and tissue background (ROI2) captured at excitation/emission wavelengths of 550/605 nm, as compared to tissue background (dashed line). (f) Spectral analysis curves of individual curcumin-labeled A β plaque, at excitation wavelength of 550 nm, as compared to tissue background (dashed line). (g) Representative image of single retinal A β plaque (ROI1) and background (ROI2) after staining with Cy5-antibody 11A5-B10 conjugate captured at excitation/emission wavelengths of 640/675 nm. (h) Spectral analysis curves of individual Cy5-antibody-labeled A β plaque, at excitation wavelength of 640 nm, as compared to tissue background (dashed line). (i and j) Representative image and spectra curves of retinal A β plaque double labeled with curcumin (ROI1; orange line) and Cy5-antibody 11A5-B10 conjugate (ROI2; purple line), and corresponding background areas (ROI3 and ROI4; dashed lines), at excitation wavelengths of 550 nm (for curcumin spectra) and 640 nm (for Ab-Cy5 conjugate). Peak wavelengths for curcumin and Cy5-antibody captured in the same individual A β plaque are distinct and separable; they remain the same as after single stainings. (k–m) Whole-mount retinas from AD patients and normal control stained with curcumin and 4G8; (k and l) A β plaques indicated by asterisks show a single-globular compacted morphology. DAPI stains nuclei. (l) Higher magnification image of an extracellular A β plaque with compacted morphology. (m) No A β plaques were detected in retinas from normal controls.

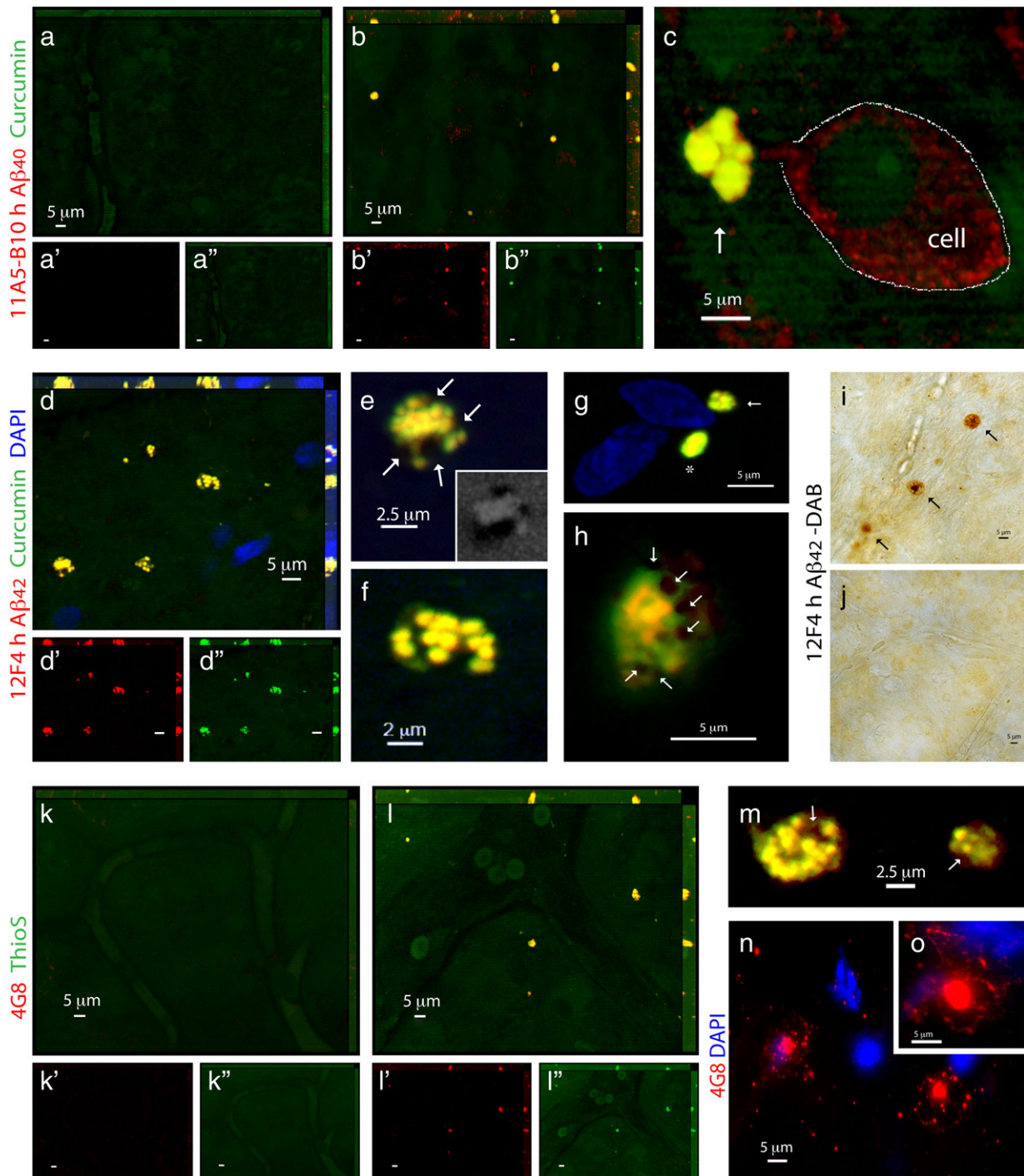


Fig. 6. Characterization of retinal A β plaques identified in postmortem retinas of definite AD patients. (a–c) Representative z-axis projection images of whole-mounted retinas of (a) normal individual compared to (b and c) AD patients following curcumin and anti-human A β_{40} mAb 11A5-B10 stainings. (a) No A β plaques could be detected in normal control retinas, whereas (b) clearly found in retinas from AD patients. (a'–b'') Separate channels for each staining. (c) At higher magnification, extracellular A β plaque with compacted large cluster is indicated by an arrow (intracellular A β_{40} is demarcated by a dotted line). (d–h) Whole-mounted retinas from AD patients stained with curcumin and anti-human A β_{42} mAb 12F4. (d' and d'') Separate channels. Note co-localization of curcumin and antibody. (e and f) Higher magnification images of A β plaques demonstrated their compacted morphology, consisting of multiple small dense cores connected in larger cluster. (e) A β plaques containing lipid deposits indicated by arrows; right bottom image captured in DAPI channel shows dark spots of SBB staining representing lipid deposits associated with retinal A β plaque. (g) A β plaques stained with curcumin and 12F4 mAb, display either compacted single-globular (asterisk) or cluster (arrow) morphology, both lack notable lipid-associated deposits. (h) A β plaque with compacted morphology and associated dark SBB staining spots suggesting the presence of lipid deposits (arrows). (i and j) Immunoperoxidase staining of A β plaques labeled with primary mAb 12F4 (plaques are indicated by black arrows) in retinal whole-mount from (i) AD patient and (j) non-AD control. DAB was used as a chromogen. (k–m) Representative retinas from (k) normal individual compared to (l) AD patient stained with ThioS and anti-A β mAb 4G8. ThioS- and 4G8 double-positive parenchymal A β plaques are found in AD patients' retinas but not in normal controls. (k'–l'') Separate channels. (m) Higher magnification demonstrating compacted morphology of ThioS-positive retinal A β plaques in AD patients' retinas (arrows indicate lipid deposits). (n and o) Single-labeled A β plaques using 4G8 mAb (secondary Ab-Cy5 conjugate) in the retinal innermost layers: A β plaques have classical morphology consisting of a central dense core and radiating fibrillar arms.

based image segmentation (using software that translated output into pseudocolor-classified digital images), “true” (unmixed) signals from curcumin-labeled A β plaques were easily distinguishable from those

generated by the blood vessels (Fig. S3c). These results indicated that the detected curcumin fluorescence signal was specific to labeled A β plaques and not due to non-specific background emission.

Identification of A β plaques in retinal samples from AD patients

The *in vivo* detection of retinal A β plaques via curcumin in live AD-Tg mice prompted us to look for their existence in human retinas from AD patients. To this end, postmortem eyes from patients with definite diagnosis of AD and age-matched non-AD controls were used (human donors are summarized in Table S1). To overcome challenges of identifying retinal A β plaques it was essential to (1) remove the vitreous, (2) eliminate autofluorescence and non-specific signals, observed in the excitation range of 360–710 nm and associated with lipofuscin/lipid deposits and long-term formalin fixation (Baschong et al., 2001; Schnell et al., 1999) by Sudan Black B (SBB) treatment, and (3) use a high-resolution optical imaging (Figs. 5–7). Following SBB treatment and curcumin staining, plaques were identified in whole-mounted retinas from AD patients (Fig. 5b and d), whereas none were detected at the same location in the absence of curcumin (Fig. 5a and c).

To ensure that each fluorochrome, when bound to A β plaques, had its distinct emission characteristic properly captured, we conducted spectral analyses of individual plaques when single-stained with curcumin (Fig. 5e) or with anti-A β_{40} antibody (with secondary-Cy5; Fig. 5g), and when co-stained with both (Fig. 5i). Regions of interest

(ROI; plaques or background) were marked, and their corresponding signal intensity was measured at increasing emission wavelengths (560–750 nm) to determine the optimal wavelength range for the excitation and capture of the distinct emission signal of each fluorochrome compared to the background (Fig. 5f, h and j). The optimal excitation for curcumin bound to A β plaques was at 550 nm, with emission peaking at 605–610 nm (Fig. 5f). The optimal excitation for Cy5-Abs bound to anti-A β mAbs attached to A β plaques was 640 nm, with emission peaking at 675 nm (Fig. 5h). DAPI staining also had a distinct spectral pattern, as expected, given its optimal excitation/emission wavelengths of 365/445 nm. Spectral analysis of double-labeled individual plaques revealed separate emission peaks for each fluorochrome (similar to the single labeling) that could be distinctly captured by our selected filter sets (Fig. 5j; see Materials and methods).

Having confirmed the ability to spectrally resolve the signals from curcumin and Cy5-labeled antibodies, we performed double staining with curcumin and several antibodies recognizing diverse epitopes within A β peptide in retinas from definite AD patients and non-AD controls (Figs. 5k–m and 6). A β plaques, positive for both curcumin and 4G8 mAb, were clearly apparent in all AD patients (Figs. 5k and l seen extracellular at higher magnification), ranging from 1 to 10 μ m

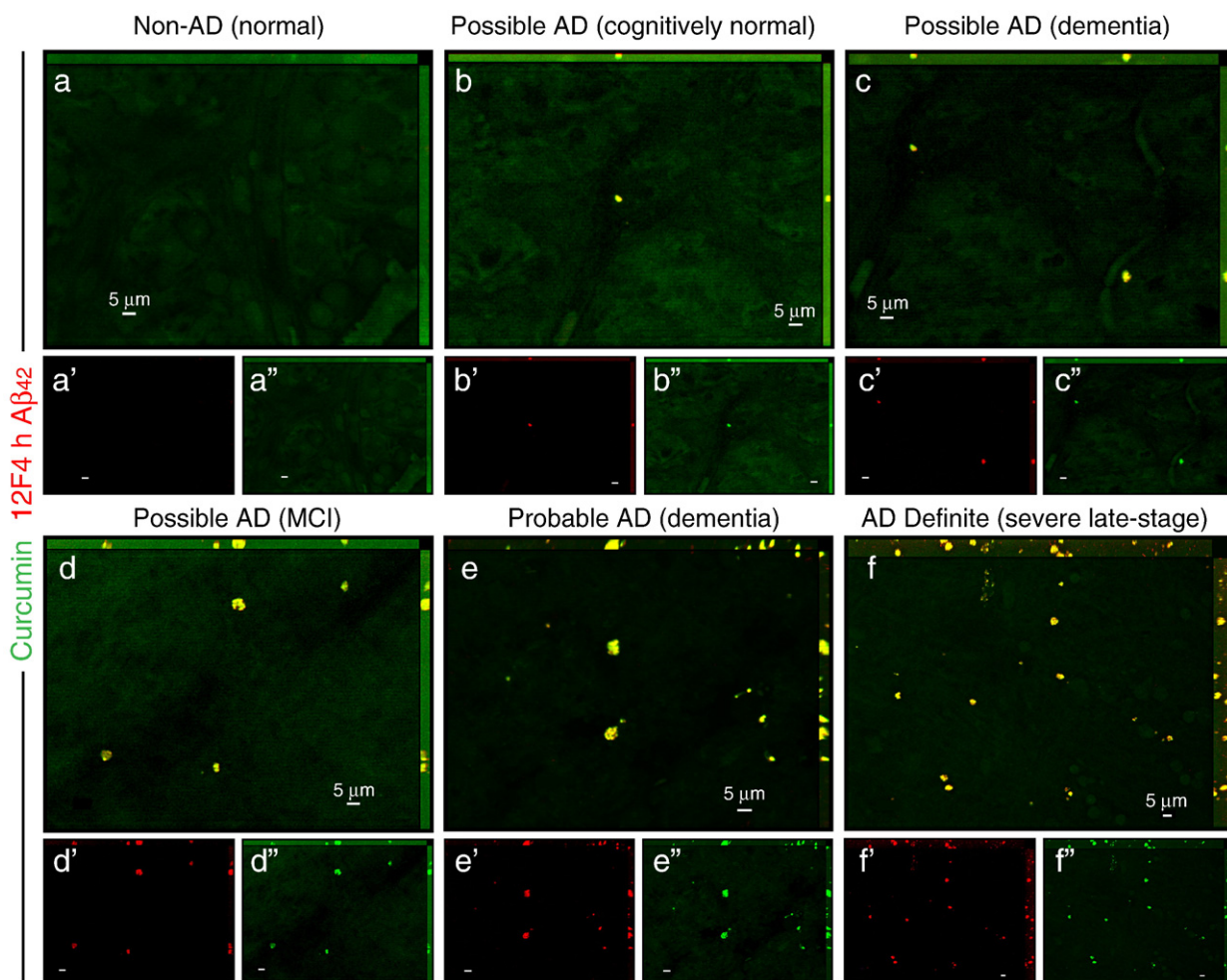


Fig. 7. Detection of retinal A β plaques in suspected early AD patients. (a–f) Representative whole-mounted retinas from normal individuals (Non-AD) and from possible/probable AD patients (based on the combined clinical diagnosis and postmortem brain pathology; Table S1), stained with curcumin and anti-A β_{42} mAb (12F4; secondary Ab-Cy5 conjugate). (a) In the retina from cognitively normal individual with no AD pathology, A β plaques could not be detected. (b) In cognitively normal individual with mild A β -plaque brain pathology (mainly diffused plaques), sparse retinal A β plaques were identified. (c and d) In patients with possible AD diagnosis, clusters of A β plaques were observed, and (e) in retinas from patients with several years of dementia and postmortem diagnosis of probable AD, A β plaques were more common throughout the retina. (f) Abundant A β plaques were observed in the retina from severe-stage AD definite patient (based on combined clinical diagnosis and postmortem brain pathology; Table S1). (a'–f'') separate channels for each staining.

in diameter (typically around 5 μm). In the retinas from control individuals stained with curcumin and 4G8, we could not detect A β plaques (Fig. 5m). To further verify the specificity of curcumin-labeled A β plaques in the human retina, we used 11A5-B10 and 12F4 mAbs recognizing the C-terminal A β_{40} and A β_{42} forms, respectively, found to be elevated in brains of AD patients (Selkoe, 2008). A β plaques could not be detected in normal control retinas stained with curcumin and anti-A β_{40} (Fig. 6a). In contrast, in the retinas from AD patients, multiple A β_{40} -containing curcumin-labeled plaques were found (Fig. 6b and c). Importantly, labeling with anti-A β_{40} revealed the presence of intracellular A β_{40} (probably its soluble form) as well as extracellular A β plaques (co-labeled with curcumin; Fig. 6c at higher magnification). Further analysis of human retinas with curcumin and anti-A β_{42} mAbs detecting the more aggregated form of A β , revealed the presence of A β_{42} -containing plaques in all samples from AD patients (Fig. 6d–h) but not from the controls (Fig. 7a). The presence of A β plaques in retinas from AD patients but not from non-AD controls was also confirmed by nonfluorescent immunoperoxidase method using anti-A β_{42} mAb and DAB as a chromogen (Fig. 6i and j).

Staining of human retinas with ThioS and anti-A β mAbs confirmed the absence of A β plaques in non-AD control samples (Fig. 6k), whereas abluminal plaques in AD patients' samples were revealed (Fig. 6l, plaques were mostly located outside the blood vessels; Fig. 6m, separate image demonstrating ThioS-positive plaques at a higher magnification). Overall, labeling patterns of retinal A β plaques by curcumin or ThioS and anti-A β mAbs, were similar in samples from AD patients and the mouse model. A diversity of A β plaque morphology was observed in retinas from AD patients: we found with a lower frequency the "classical/neuritic" plaque structure, possessing a central dense core and radiating fibrillar arms consisting of A β deposits (Fig. 6n and o), and with a higher frequency the "compacted" ("burned-out") plaques composed of a dense core globular amyloid deposit with no apparent radiating fibrils. Compacted plaques had either a single core (Figs. 5k and l and 6g) or clusters: consisting of few dense cores in a cluster (Fig. 6b, c and g) or multiple small dense cores connected to each other in a relatively large core (Fig. 6d–f and l–m). Some A β plaques included lipid deposits stained in dark color by SBB (Fig. 6e, h and m), which may entail their pathological impact based on recent report demonstrating the neurotoxicity of the lipid-containing plaques (Martins et al., 2008). It should be noted that classical plaque structure seemed more common in the brains from AD patients than in their respective retinas, and that the fibrillary arms were clearly positive for anti-A β Abs whereas less intensely stained with curcumin (Fig. S4a–c). Very similar plaque structures were observed in AD-Tg mouse brains stained with curcumin or ThioS and co-labeled with A β mAbs, with the same distinctive patterns for each staining method as seen in human brains; a reflection of the recognized epitopes (Fig. S4d–f). Curcumin, similar to ThioS, binds to A β plaque structure rather than a specific sequence, and intensely stains the central dense core. It is also suggested that the dense core A β plaques seen in AD patients' retinas are formed at early stages of the disease, considering the "life pathogenesis" hypothesis for development of different plaque types (Armstrong, 1998).

Detection of A β plaques in retinal samples from suspected early stage AD patients

A β plaques, positively stained with curcumin, were further detected in postmortem retinas from suspected AD patients that were possibly at early disease stages (Fig. 7). These included a group of individuals that could be identified as early stage AD (Morris and Price, 2001), based on their combined clinical diagnosis and postmortem brain neuropathology: patients with few years of dementia suspected for possible or probable AD diagnosis, a patient with mild cognitive impairment (MCI) that had higher probability to

develop AD (Petersen et al., 1999), and a preclinical individual with postmortem detection of initial A β plaque pathology in the brain (Table S1, patients #9–13). We found a qualitative correlation between the severities of the clinical diagnosis verified by postmortem neuropathology and retinal A β plaque burden (Fig. 7b–f). Overall, we were able to identify A β plaques, which were specifically detected with curcumin, in the retinas from definite and suspected early AD patients.

Discussion

The present study demonstrates that a noninvasive *in vivo* monitoring of AD hallmark pathology via optical imaging with high specificity and resolution is feasible through the retina. Two key issues towards translation of this approach for the detection of Alzheimer's in humans have been accomplished here: *in vivo* imaging of A β plaques in the retina of live AD animals, and identification of amyloid plaques in retinas from human Alzheimer's disease patients, even before clinical symptoms allow disease diagnosis with certainty, thereby creating the basis for developing an early diagnostic marker specific to Alzheimer's disease.

The detection of retinal A β plaques in suspected patients is important, as previous reports indicated that a considerable percentage of these patients suffering from mild dementia and/or MCI (exhibiting memory impairments but not fully demented) will develop AD (Morris and Price, 2001; Petersen et al., 1999). Moreover, we were able to identify A β plaques in the retina from a cognitively normal individual who had sparsely diffused plaques in the hippocampus discovered only after brain autopsy.

Neuropathological abnormalities associated with AD, especially A β alterations (Jack et al., 2010), may occur during the prodromal phase, as early as decades before the clinical phase of full disease manifestation. Therefore, there is a need for early diagnosis allowing early intervention, in order to achieve an efficient response to therapy (Holmes et al., 2008). In this respect, our data from AD mouse model on the detection of A β plaques via curcumin in the retina before they become visible in the brain, and plaque burden correlation with the progression of brain pathology, appear encouraging. Moreover, the significant reduction of A β plaques observed in retinas from AD mice following immunization with myelin-derived peptide supports our contention that retinal plaque pathology faithfully represents the brain disease and encourages the development of retinal imaging via curcumin for monitoring AD plaques and assessment of response to therapies.

Retinal A β plaques in our postmortem samples from AD patients were detected mostly within the inner layers, which makes live imaging/screening of potential patients' retinas a feasible strategy, most likely through improvement of available ophthalmoscopy tools, by the addition of adaptive optics (Carroll et al., 2008) and spectral imaging. Although the current human study has a relatively limited sample size, our results provide, for the first time, a proof for the existence of amyloid plaque pathology in the retina that is specific to Alzheimer's disease. In addition, these data may form the basis for a more quantitative clinical trial. Importantly, the bioavailability of curcumin to the mouse eye following its systemic injection and its high affinity to A β plaques enabled the detection of these plaques in live animals. In terms of safety, Phase I and II trials using curcumin in patients with cancer have proven its low toxicity in humans even at high doses (12 g/day), and when given over extended periods of time (Dhillon et al., 2008). Translation of curcumin doses given intravenously or orally from mice to humans (<1 g) for retinal plaque visualization is expected to remain within the determined safety levels. Furthermore, recent studies have reported various approaches to significantly increase curcumin stability and bioavailability in humans (Anand et al., 2007).

A β plaques in retinas from AD patients appear to be a specific diagnostic marker as compared to the previously described early visual dysfunctions (Katz and Rimmer, 1989; Sadun et al., 1987) and retinal abnormalities, especially atrophy of the NFL (Berisha et al., 2007; Blanks et al., 1996; Hinton et al., 1986; Trick et al., 1989), which were also evident in other eye disorders and neurodegenerative conditions (Jindahra et al., 2010; Parisi, 2003). Moreover, based on their unique size, signature and distribution within the retinas, A β plaques observed in AD patients could be eventually used for differential diagnosis. For instance, plaques detected in age-related macular degeneration are locally restricted to retinal pigment epithelium within drusen and appear smaller in size (Anderson et al., 2004). In glaucoma, NFL and GCL are altered, and increased intracellular expression of A β was found in RGCs in a rat model (Guo et al., 2007), but no A β plaques were detected in glaucoma patients or animal models.

Conclusions

This study provides the first demonstration of A β plaques in postmortem retinas from suspected and definite AD patients that reflected AD brain pathology. In addition, systemic administration of curcumin to AD mice resulted in specific *in vivo* labeling of retinal A β plaques. This novel approach enabled noninvasive and high-resolution monitoring of individual retinal A β plaques in live AD mice. Finally, curcumin-visualized retinal plaques were shown to decrease in number and size following immunization with altered myelin-derived peptide, with dynamics and extent similar to their brain counterparts in an animal model. The reported data thus provide the basis for direct noninvasive optical imaging of AD plaque pathology through the retina with high resolution and sensitivity. Future studies are required to demonstrate the ability to detect A β plaques in the retinas of live AD patients for disease diagnosis and monitoring.

Competing interests statement

The authors declare that no conflict of interest exists.

Acknowledgments

We thank Drs. J.Y. Hwang, Y. Kohanzadeh, A.G. Nowatzyk, K.V. Ramanujan and K. Wawrowsky for useful discussions and imaging collaboration. M.S. holds the Maurice and Ilse Katz Professorial Chair in Neuroimmunology at The Weizmann Institute of Science, Israel. This work was supported in part by the Marciano Family Foundation, the U.S. Navy Bureau of Medicine and Surgery, R01 EY13431 and M01 RR00425, the Winnick Family Foundation, and the University of Southern California Alzheimer's Disease Research Center NIA P50 AG05142. We also thank IBMISPS for the opportunity to publish in its special issue.

Appendix A. Supplementary data

Supplementary data associated with this article can be found, in the online version, at doi:10.1016/j.neuroimage.2010.06.020.

References

- Anand, P., Kunnumakkara, A.B., Newman, R.A., Aggarwal, B.B., 2007. Bioavailability of curcumin: problems and promises. *Mol. Pharm.* 4, 807–818.
- Anderson, D.H., Talaga, K.C., Rivest, A.J., Barron, E., Hageman, G.S., Johnson, L.V., 2004. Characterization of β amyloid assemblies in drusen: the deposits associated with aging and age-related macular degeneration. *Exp. Eye Res.* 78, 243–256.
- Armstrong, R.A., 1998. β -Amyloid plaques: stages in life history or independent origin? *Dement. Geriatr. Cogn. Disord.* 9, 227–238.
- Baschong, W., Suetterlin, R., Laeng, R.H., 2001. Control of autofluorescence of archival formaldehyde-fixed, paraffin-embedded tissue in confocal laser scanning microscopy (CLSM). *J. Histochem. Cytochem.* 49, 1565–1572.
- Berisha, F., Feke, G.T., Trempe, C.L., McMeel, J.W., Schepens, C.L., 2007. Retinal abnormalities in early Alzheimer's disease. *Invest. Ophthalmol. Vis. Sci.* 48, 2285–2289.
- Blanks, J.C., Torigoe, Y., Hinton, D.R., Blanks, R.H., 1996. Retinal pathology in Alzheimer's disease I. Ganglion cell loss in foveal/parafoveal retina. *Neurobiol. Aging* 17, 377–384.
- Burton, K., Jeong, J., Wachsmann-Hogiu, S., Farkas, D.L., 2009. Spectral optical imaging in biology and medicine. In: *Biomedical Optical Imaging*. Oxford University Press. ISBN: 978-0-19-515044-5.
- Carroll, J., Choi, S.S., Williams, D.R., 2008. *In vivo* imaging of the photoreceptor mosaic of a rod monochromat. *Vis. Res.* 48, 2564–2568.
- Cordeiro, M.F., Guo, L., Coxon, K.M., Duggan, J., Nizari, S., Normando, E.M., Sensi, S.L., Sillito, A.M., Fitzke, F.W., Salt, T.E., Moss, S.E., 2010. Imaging multiple phases of neurodegeneration: a novel approach to assessing cell death *in vivo*. *Cell Death Dis.* 1, 1–11.
- Dhillon, N., Aggarwal, B.B., Newman, R.A., Wolff, R.A., Kunnumakkara, A.B., Abbruzzese, J.L., Ng, C.S., Badmaev, V., Kurzrock, R., 2008. Phase II trial of curcumin in patients with advanced pancreatic cancer. *Clin. Cancer Res.* 14, 4491–4499.
- Ford, M.L., Evavold, B.D., 2004. An MHC anchor-substituted analog of myelin oligodendrocyte glycoprotein 35–55 induces IFN- γ and autoantibodies in the absence of experimental autoimmune encephalomyelitis and optic neuritis. *Eur. J. Immunol.* 34, 388–397.
- Fujimoto, J.G., Farkas, D.L. (Eds.), 2009. *Biomedical Optical Imaging*. Oxford University Press. ISBN: 978-0-19-515044-5.
- Garcia-Alloza, M., Robbins, E.M., Zhang-Nunes, S.X., Purcell, S.M., Betensky, R.A., Raju, S., Prada, C., Greenberg, S.M., Bacskai, B.J., Frosch, M.P., 2006. Characterization of amyloid deposition in the APPsw/PS1E9 mouse model of Alzheimer disease. *Neurobiol. Dis.* 24, 516–524.
- Garcia-Alloza, M., Borrelli, L.A., Rozkalne, A., Hyman, B.T., Bacskai, B.J., 2007. Curcumin labels amyloid pathology *in vivo*, disrupts existing plaques, and partially restores distorted neurites in an Alzheimer mouse model. *J. Neurochem.* 102, 1095–1104.
- Goldstein, L.E., Muffat, J.A., Cherny, R.A., Moir, R.D., Ericsson, M.H., Huang, X., Mavros, C., Coccia, J.A., Faget, K.Y., Fitch, K.A., Masters, C.L., Tanzi, R.E., Chylack Jr., L.T., Bush, A.I., 2003. Cytosolic β -amyloid deposition and supranuclear cataracts in lenses from people with Alzheimer's disease. *Lancet* 361, 1258–1265.
- Guo, L., Salt, T.E., Luong, V., Wood, N., Cheung, W., Maass, A., Ferrari, G., Russo-Marie, F., Sillito, A.M., Cheetham, M.E., Moss, S.E., Fitzke, F.W., Cordeiro, M.F., 2007. Targeting amyloid- β in glaucoma treatment. *Proc. Natl. Acad. Sci. U. S. A.* 104, 13444–13449.
- Hardy, J., Selkoe, D.J., 2002. The amyloid hypothesis of Alzheimer's disease: progress and problems on the road to therapeutics. *Science* 297, 353–356.
- Hintersteiner, M., Enz, A., Frey, P., Jatou, A.L., Kinzy, W., Kneuer, R., Neumann, U., Rudin, M., Staufenbiel, M., Stoekli, M., Wiederhold, K.H., Gremlich, H.U., 2005. *In vivo* detection of amyloid- β deposits by near-infrared imaging using an oxazine-derivative probe. *Nat. Biotechnol.* 23, 577–583.
- Hinton, D.R., Sadun, A.A., Blanks, J.C., Miller, C.A., 1986. Optic-nerve degeneration in Alzheimer's disease. *N Engl J. Med.* 315, 485–487.
- Holmes, C., Boche, D., Wilkinson, D., Yadegarfar, G., Hopkins, V., Bayer, A., Jones, R.W., Bullock, R., Love, S., Neal, J.W., Zotova, E., Nicoll, J.A., 2008. Long-term effects of A β ₄₂ immunisation in Alzheimer's disease: follow-up of a randomised, placebo-controlled phase I trial. *Lancet* 372, 216–223.
- Jack Jr., C.R., Knopman, D.S., Jagust, W.J., Shaw, L.M., Aisen, P.S., Weiner, M.W., Petersen, R.C., Trojanowski, J.Q., 2010. Hypothetical model of dynamic biomarkers of the Alzheimer's pathological cascade. *Lancet Neurol.* 9, 119–128.
- Jankowsky, J.L., Fadale, D.J., Anderson, J., Xu, G.M., Gonzales, V., Jenkins, N.A., Copeland, N.G., Lee, M.K., Younkin, L.H., Wagner, S.L., Younkin, S.G., Borchelt, D.R., 2004a. Mutant presenilins specifically elevate the levels of the 42 residue β -amyloid peptide *in vivo*: evidence for augmentation of a 42-specific γ secretase. *Hum. Mol. Genet.* 13, 159–170.
- Jankowsky, J.L., Slunt, H.H., Gonzales, V., Jenkins, N.A., Copeland, N.G., Borchelt, D.R., 2004b. APP processing and amyloid deposition in mice haplo-insufficient for presenilin 1. *Neurobiol. Aging* 25, 885–892.
- Jindahra, P., Hedges, T.R., Mendoza-Santesteban, C.E., Plant, G.T., 2010. Optical coherence tomography of the retina: applications in neurology. *Curr. Opin. Neurol.* 23, 16–23.
- Katz, B., Rimmer, S., 1989. Ophthalmologic manifestations of Alzheimer's disease. *Surv. Ophthalmol.* 34, 31–43.
- Klunk, W.E., Engler, H., Nordberg, A., Wang, Y., Blomqvist, G., Holt, D.P., Bergstrom, M., Savitcheva, I., Huang, G.F., Estrada, S., Ausen, B., Debnath, M.L., Barletta, J., Price, J.C., Sandell, J., Lopresti, B.J., Wall, A., Koivisto, P., Antoni, G., Mathis, C.A., Langstrom, B., 2004. Imaging brain amyloid in Alzheimer's disease with Pittsburgh Compound-B. *Ann. Neurol.* 55, 306–319.
- Klunk, W.E., Lopresti, B.J., Ikonomic, M.D., Lefterov, I.M., Koldamova, R.P., Abrahamson, E.E., Debnath, M.L., Holt, D.P., Huang, G.F., Shao, L., DeKosky, S.T., Price, J.C., Mathis, C.A., 2005. Binding of the positron emission tomography tracer Pittsburgh compound-B reflects the amount of amyloid- β in Alzheimer's disease brain but not in transgenic mouse brain. *J. Neurosci.* 25, 10598–10606.
- Koronyo-Hamaoui, M., Ko, M.K., Koronyo, Y., Azoulay, D., Seksenyan, A., Kunis, G., Pham, M., Bakhsheshian, J., Rogeri, P., Black, K.L., Farkas, D.L., Schwartz, M., 2009. Attenuation of AD-like neuropathology by harnessing peripheral immune cells: local elevation of IL-10 and MMP-9. *J. Neurochem.* 111, 1409–1424.
- Lockhart, A., Lamb, J.R., Osredkar, T., Sue, L.I., Joyce, J.N., Ye, L., Libri, V., Leppert, D., Beach, T.G., 2007. PIB is a non-specific imaging marker of amyloid-beta (A β) peptide-related cerebral amyloidosis. *Brain* 130, 2607–2615.
- Martins, I.C., Kuperstein, I., Wilkinson, H., Maes, E., Vanbrabant, M., Jonckheere, W., Van Gelder, P., Hartmann, D., D'Hooge, R., De Strooper, B., Schymkowitz, J., Rousseau, F.,

2008. Lipids revert inert A β amyloid fibrils to neurotoxic protofibrils that affect learning in mice. *EMBO J.* 27, 224–233.
- McGeer, P.L., McGeer, E.G., 2002. Local neuroinflammation and the progression of Alzheimer's disease. *J. Neurovirol.* 8, 529–538.
- Meyer-Luehmann, M., Spires-Jones, T.L., Prada, C., Garcia-Alloza, M., de Calignon, A., Rozkalne, A., Koenigsknecht-Talboo, J., Holtzman, D.M., Bacskai, B.J., Hyman, B.T., 2008. Rapid appearance and local toxicity of amyloid- β plaques in a mouse model of Alzheimer's disease. *Nature* 451, 720–724.
- Mirra, S.S., Heyman, A., McKeel, D., Sumi, S.M., Crain, B.J., Brownlee, L.M., Vogel, F.S., Hughes, J.P., van Belle, G., Berg, L., 1991. The Consortium to Establish a Registry for Alzheimer's Disease (CERAD) Part II. Standardization of the neuropathologic assessment of Alzheimer's disease. *Neurology* 41, 479–486.
- Morris, J.C., Price, A.L., 2001. Pathologic correlates of nondemented aging, mild cognitive impairment, and early-stage Alzheimer's disease. *J. Mol. Neurosci.* 17, 101–118.
- Nakada, T., Matsuzawa, H., Igarashi, H., Fujii, Y., Kwee, I.L., 2008. In vivo visualization of senile-plaque-like pathology in Alzheimer's disease patients by MR microscopy on a 7 T system. *J. Neuroimaging* 18, 125–129.
- Ng, S., Villemagne, V.L., Berlangieri, S., Lee, S.T., Cherk, M., Gong, S.J., Ackermann, U., Saunderson, T., Tochon-Danguy, H., Jones, G., Smith, C., O'Keefe, G., Masters, C.L., Rowe, C.C., 2007. Visual assessment versus quantitative assessment of ^{11}C -PIB PET and ^{18}F -FDG PET for detection of Alzheimer's disease. *J. Nucl. Med.* 48, 547–552.
- Ning, A., Cui, J.Z., To, E., Hsiao Ashe, K., Matsubara, J.A., 2008. Amyloid- β deposits lead to retinal degeneration in a mouse model of Alzheimer disease. *Invest. Ophthalmol. Vis. Sci.* 49, 5136–5143.
- Parisi, V., 2003. Correlation between morphological and functional retinal impairment in patients affected by ocular hypertension, glaucoma, demyelinating optic neuritis and Alzheimer's disease. *Semin. Ophthalmol.* 18, 50–57.
- Perez, S.E., Lumayag, S., Kovacs, B., Mufson, E.J., Xu, S., 2009. β -Amyloid deposition and functional impairment in the retina of the APP^{swe}/PS1 ΔE9 transgenic mouse model of Alzheimer's disease. *Invest. Ophthalmol. Vis. Sci.* 50, 793–800.
- Petersen, R.C., Smith, G.E., Waring, S.C., Ivnik, R.J., Tangalos, E.G., Kokmen, E., 1999. Mild cognitive impairment: clinical characterization and outcome. *Arch. Neurol.* 56, 303–308.
- Sadun, A.A., Borchert, M., DeVita, E., Hinton, D.R., Bassi, C.J., 1987. Assessment of visual impairment in patients with Alzheimer's disease. *Am. J. Ophthalmol.* 104, 113–120.
- Schnell, S.A., Staines, W.A., Wessendorf, M.W., 1999. Reduction of lipofuscin-like autofluorescence in fluorescently labeled tissue. *J. Histochem. Cytochem.* 47, 719–730.
- Selkoe, D.J., 2008. Soluble oligomers of the amyloid β -protein impair synaptic plasticity and behavior. *Behav. Brain Res.* 192, 106–113.
- Sisodia, S.S., Price, D.L., 1995. Role of the β -amyloid protein in Alzheimer's disease. *FASEB J.* 9, 366–370.
- Toyama, H., Ye, D., Ichise, M., Liow, J.S., Cai, L., Jacobowitz, D., Musachio, J.L., Hong, J., Crescenzo, M., Tipre, D., Lu, J.Q., Zoghbi, S., Vines, D.C., Seidel, J., Katada, K., Green, M.V., Pike, V.W., Cohen, R.M., Innis, R.B., 2005. PET imaging of brain with the β -amyloid probe, [^{11}C]6-OH-BTA-1, in a transgenic mouse model of Alzheimer's disease. *Eur. J. Nucl. Med. Mol. Imaging* 32, 593–600.
- Trick, G.L., Barris, M.C., Bickler-Bluth, M., 1989. Abnormal pattern electroretinograms in patients with senile dementia of the Alzheimer type. *Ann. Neurol.* 26, 226–231.
- Wachman, E.S., Niu, W., Farkas, D.L., 1997. AOTF microscope for imaging with increased speed and spectral versatility. *Biophys. J.* 73, 1215–1222.
- Wyss-Coray, T., 2006. Inflammation in Alzheimer disease: driving force, bystander or beneficial response? *Nat. Med.* 12, 1005–1015.
- Yang, F., Lim, G.P., Begun, A.N., Ubeda, O.J., Simmons, M.R., Ambegaokar, S.S., Chen, P.P., Kaye, R., Glabe, C.G., Frautschi, S.A., Cole, G.M., 2005. Curcumin inhibits formation of amyloid β oligomers and fibrils, binds plaques, and reduces amyloid *in vivo*. *J. Biol. Chem.* 280, 5892–5901.
- Ziv, Y., Avidan, H., Pluchino, S., Martino, G., Schwartz, M., 2006. Synergy between immune cells and adult neural stem/progenitor cells promotes functional recovery from spinal cord injury. *Proc. Natl. Acad. Sci. U. S. A.* 103, 13174–13179.